AUGMENTING INTENSITY TO ENHANCE SCENE STRUCTURE IN PROSTHETIC VISION

Chris McCarthy, David Feng and Nick Barnes*

Computer Vision Research Group, NICTA, Canberra ACT, Australia
College of Engineering and Computer Science, Australian National University, Canberra ACT, Australia
{cmccarthy,dfeng,nmb}@nicta.com.au

ABSTRACT

We present a novel visual representation for prosthetic vision that augments intensity in order to emphasise regions of structural change. This is achieved via the adaptation of a recently proposed method for measuring the extent of local variation of surface orientation in corresponding disparity images. The proposed visual representation demonstrates how intensity and depth data may be combined to provide a scene representation that shows visual appearance as brightness in the familiar way (*i.e.*, intensity-based), but ensures structurally important features such as steps, doorways and drop-offs, as well as general items of interest remain perceivable, regardless of contrast. Qualitative comparisons of the proposed visual representation in simulated prosthetic vision (98 phosphenes) suggest potential advantages over non-augmented intensity for distinguishing between free and obstructed space in the scene, and for perceiving features of interest on smooth surfaces.

***Index Terms*—** prosthetic vision, image processing, low vision, mobility and orientation

1. INTRODUCTION

Interest in prosthetic vision has grown significantly in the last ten years [1, 2, 3, 4, 5]. In particular, retinal prostheses have developed significantly, with some now undergoing human trials (*e.g.*, [3, 4]). These devices aim to restore the sense of vision in those who have lost sight through retinal degenerative diseases such as Retinitis Pigmentosa and Age-related Macular Degeneration [6]. Retinal prostheses artificially stimulate the remaining cells, and in particular retinal ganglion cells that interface with the optic nerve. This is achieved via electrical pulses delivered by an implanted array of electrodes near the retina. The elicited response experienced by implantees is an image made up of *phosphenes* [7]. Phosphenes are typically described by patients as bright spots of light, each loosely corresponding to one stimulating electrode. Studies have shown that the brightness and/or size of phosphenes can often increase with changes in stimulation parameters [8, 9]. These studies show up to around 10 levels of intensity can be differentiated by implantees. This allows induced images to be rendered by modulating stimulus parameters delivered by each electrode [7, 4, 3].

The dominant approach for capturing scene data is via an externally worn camera. While other approaches exist (*e.g.*, [4]), a particular advantage of capturing image data externally is that vision processing may then be performed to extract information most relevant to the needs of perception, and the task. This is important because current and near-term retinal prostheses are severely limited in the visual information they can convey; in particular, resolution and dynamic range. This motivates consideration of how vision processing may be used to construct visual representations that better facilitate functional outcomes for implantees.

Enabling safe and efficient mobility is a primary aim of retinal prostheses. Mobility studies with prosthetic vision to date have primarily focussed on basic way-finding tasks using simulated prosthetic vision (SPV), typically in high contrast, black-and-white environments [10, 11, 12, 13, 14, 15]. Dagnelie *et al.* [11] examine the effects of reduced resolution, low dynamic range and phosphene image degradation on mobility in a sparsely obstructed and controlled indoor environment. Parikh *et al.* [14] show the effective use of peripheral cueing from a visual saliency algorithm [16] to assist mobility using simulated phosphene vision. Pradeep *et al.* [17] describe the use of stereo vision to detect obstacles and estimate safe and efficient paths in the scene. Recent SPV studies have also examined the use of depth as an alternative mode of representation [18]. In [19] depth is extended to an augmented-depth representation whereby obstacles on the ground are made brighter relative to the floor.

Given the constraints of current and near-term visual prostheses, there is sound motivation to explore alternative modes

*The authors acknowledge the contributions of Paulette Lieby, Adele Scott, Ashley Stacey, Jeremy Oorloff and Nathan Gough, authors of the simulated prosthetic vision software: lucid, used in this paper. C. McCarthy also acknowledges time spent at the Centre for Eye Research Australia (CERA), the Bionics Institute, and the Centre for Neural Engineering at The University of Melbourne, where some of this research was conducted, and image data acquired. This research was supported by the Australian Research Council (ARC) through its Special Research Initiative (SRI) in Bionic Vision Science and Technology grant to Bionic Vision Australia (BVA). NICTA is funded by the Australian Government as represented by the Department of Broadband, Communications and the Digital Economy and the Australian Research Council through the ICT Centre of Excellence program.

of scene representation, particularly in low-contrast conditions. However, such visual representations are designed specifically for the needs of safe mobility, and do not readily generalise to other tasks. This motivates consideration of how an intensity-based visual representation may be enhanced in order to emphasise potentially hazardous low-contrast surface boundaries and/or small trip hazards, while still retaining as many of the natural features of the scene as possible.

In this paper we propose a new visual representation for prosthetic vision that augments the intensity image in order to emphasise scene structure in the resulting visual representation. Assuming an RGB-D sensor, we adapt a recently proposed method for estimating the extent of surface orientation change (referred to as a *perturbance map*). By combining the resulting map with the intensity image, features of structural interest are emphasised relative to less interesting dominant surfaces such as the ground, walls, and table-tops. Our approach is real-time, removes assumptions of high-contrast environments, and is achieved without parameterised surface modelling. We qualitatively compare our approach with non-augmented intensity over a range of simulated prosthetic vision images portraying typical activities of daily living, as well as potentially hazardous mobility scenarios.

The paper is structured as follows. Section 2 introduces our proposed visual representation for prosthetic vision, and provides details of how the perturbance map is computed. Section 3 presents qualitative data showing the output of our proposed augmentation, as well as a comparison against non-augmented intensity using simulated prosthetic vision. Section 4 provides a brief discussion of our results, and Section 5, our conclusions.

2. AUGMENTING INTENSITY TO ENHANCE SCENE STRUCTURE

The proposed visual representation seeks to balance the needs of emphasising scene structure unambiguously, while simultaneously conveying as much of the naturally occurring intensity function as possible. We thus propose scaling the original intensity image, $I(\mathbf{p}) \in \mathbb{R}$, by the estimated extent of local structural change (relative to the surroundings) at each image location such that:

$$I^*(\mathbf{p}) = \lambda \mathcal{P}(\mathbf{p}) I(\mathbf{p}), \tag{1}$$

where λ is a scale factor determining the final brightness of the scene, and $\mathcal{P} \in [0, 1]$ is the estimated structural perturbance. The effect is to reduce the intensity of regions of low structural change (*e.g.*, large smooth surfaces such as the ground plane, walls and table-tops) in order to increase the contrast of more structurally interesting regions in the scene.

2.1. Implementation

The proposed augmentation requires a normalised map of structural change across the image. For this we modify our recently proposed algorithm for estimating regions of surface orientation change in a disparity image [20]. The original algorithm operates on extracted iso-disparity contours. Here we propose an equivalent implementation of the concept using disparity gradients. We detail our implementation of the method below.

2.1.1. Surface orientation perturbance

The algorithm computes the perturbance map $\mathcal{P}$ for an input dense disparity frame $D \in \mathbb{R}$. The three main steps of the algorithm are listed in 2.1.2, 2.1.3, and 2.1.4, and a method of handling non-dense input is presented in 2.1.5.

2.1.2. Multi-Scale Histogramming of Disparity Gradient Orientation

Firstly, a sliding window approach is utilised to quantify the characteristics of the local neighbourhood of each pixel. For each window, the disparity image gradient orientations of contained pixels are counted into a number of discrete histogram bins. The orientation histogram of the window of scale s at position $\mathbf{p} \in D$ is denoted as $H_{s,\mathbf{p}} : [1..B] \rightarrow \mathbb{R}_{>0}$, where B (set to 9 in the implementation) is the total number of orientation bins.

2.1.3. Fixed-Scale Perturbance Computation

The fixed-scale cost between two windows, at positions $\mathbf{p}$ and $\mathbf{p}'$ is defined by the following function:

$$C_s(\mathbf{p}, \mathbf{p}') = \log\left(1 + \frac{\sum_{b=1}^{B} \left| H_{s,\mathbf{p}}(b) - H_{s,\mathbf{p}'}(b) \right|}{\sum_{b=1}^{B} \max\left(H_{s,\mathbf{p}}(b), H_{s,\mathbf{p}'}(b)\right)}\right), \tag{2}$$

where $\max$ returns the histogram with the largest bin, and the subscript s again refers to the scale.

The fixed-scale perturbance of a pixel $\mathbf{p}$ is defined as a weighted average of the costs between its window and the windows of the pixels in a neighbourhood of radius r (set to 2 in the implementation). It is given by the formula

$$\mathcal{P}_s(\mathbf{p}, r) = \frac{\sum_{\mathbf{p}' \in N(\mathbf{p}, r)} \frac{1}{|\mathbf{p} - \mathbf{p}'|} \times C_s(\mathbf{p}, \mathbf{p}')}{\sum_{\mathbf{p}' \in N(\mathbf{p}, r)} \frac{1}{|\mathbf{p} - \mathbf{p}'|}} \tag{3}$$

where $N(\mathbf{p}, r) \subset \mathbb{R}^2$ represents the neighbourhood of $\mathbf{p}$ of radius r.

2.1.4. Multi-Scale Perturbance Combination

The computed fixed-scale perturbance images are combined into a single perturbance map by taking the average across

each window position, weighted by window occupancy. The window occupancy coefficient for a window at position $\mathbf{p}$ of scale s is defined as

$$W(\mathbf{p}, s) = \log\left(1 + \frac{O(\mathbf{p}, s)}{s^2}\right) \tag{4}$$

where $O(\mathbf{p}, s)$ denotes the number of pixels with valid gradient orientations in the window specified by $\mathbf{p}$ and s.

Thus the combined perturbance score for each pixel is given by the formula

$$\mathcal{P}(\mathbf{p}, r, S) = \frac{\sum_{s\in S} W(\mathbf{p}, s) \cdot \mathcal{P}_s(\mathbf{p}, r)}{\sum_{s\in S} W(\mathbf{p}, s)} \tag{5}$$

where $S \subset \mathbb{R}$ (set to $\{40, 50, 60\}$ in the implementation) is the set of window scales. In order to 'sharpen' areas of higher perturbance, each pixel in the final image is squared and then smoothed with a log function.

2.1.5. Modifications for Non-Dense Disparity

Real world disparity data often contains regions of missing values, which may lead to erroneous high perturbance scores around these regions. Step 2.1.3 can be modified to address this issue, by directly weighting each window's contribution with a disparity occupancy coefficient for the window, defined as:

$$Q(\mathbf{p}, s) = \left(\frac{\left|\{\mathbf{p}' \in U(p, s) : D(\mathbf{p}') \text{ not missing}\}\right|}{s \cdot s}\right)^t \tag{6}$$

where $U(p, s) \subset D$ is the window at p of scale s, and the constant t (set to 1 in the implementation) controls the level of suppression of missing disparity values. The modified fixed-scale perturbance algorithm for non-dense inputs is thus given by:

$$\mathcal{P}_s(\mathbf{p}, r) = Q(\mathbf{p}, s) \cdot \frac{\sum_{\mathbf{p}'\in N(\mathbf{p},r)} \frac{1}{|\mathbf{p}-\mathbf{p}'|} \cdot Q(\mathbf{p}', s) \cdot C_s(\mathbf{p}, \mathbf{p}')}{\sum_{\mathbf{p}'\in N(\mathbf{p},r)} \frac{1}{|\mathbf{p}-\mathbf{p}'|} \cdot Q(\mathbf{p}', s)} \tag{7}$$

2.2. Special case

Considering Equation 1, a special case exists when the input intensity is 0. In this case, the perturbance scaling has no impact, leaving open the possibility of a black object with high $\mathcal{P}(\mathbf{p})$ on a black background remaining unaltered, despite it being of clear structural interest. In general, the proposed augmentation will have less effect on objects of lower intensity; a consequence of the objective to convey as much of the naturally occurring intensity while also emphasising structural features in the scene. However, to avoid the special case of near black objects not being emphasised, we introduce the pre-processing function, $f(x)$, into Equation 1, such that:

$$I^*(\mathbf{p}) = \lambda \mathcal{P}(\mathbf{p}) f(I(\mathbf{p})), \tag{8}$$

where

$$f(x) = |x - I_{\text{min}}| + I_{\text{min}},$$

and I_{min} defines a minimum allowable intensity (set close to 0). The effect of $f(x)$ is to reflect intensities below I_{min} to be above the threshold by the same difference. Other alternatives include adding an offset to the input intensity, or setting $f(x)$ to $\max(x, I_{\text{min}})$.

3. RESULTS

To assess the proposed visual representation, a series of images were captured with an ASUS Xtion Pro RGB-D sensor. Figure 1 shows sample frames taken from a sequence around a typical office environment. The figure shows the original captured greyscale image, the output of the orientation perturbance map, and the resulting augmentation using Equation 8 ($\lambda = 2$, $I_{\text{min}} = 0.05$). It can be seen that the perturbance map successfully highlights regions of structural change such as wall-floor boundaries and clutter along the walk-way. Large smooth surfaces are clearly scaled down in intensity, thereby ensuring low-contrast connected surfaces such as between the grey cabinet and floor in Figures 1(a) and (b) are clearly highlighted in the resulting augmentation. The white boxes on the bench top in Figure 1(e) are clearly distinguishable from the white wall behind them.

Figure 2 provides examples of the proposed augmentation in the context of typical everyday scenarios. It can be seen that the perturbance detector successfully highlights potential hazards such as steps (Fig 2(b)), and drop-offs (Fig 2(c)). Close inspection of the original image in Fig 2(c) shows that the most noticeable change in intensity only occurs three steps down, highlighting the unreliability of contrast change alone to mark such events. In the resulting augmentation, however, the initial drop-off step is made evident relative to the ground surface leading up to it. The table-top example in Figure 2(e) also demonstrates the effectiveness of the augmentation for highlighting objects of interest on a planar surface.

A preliminary assessment of the comparative advantages of the proposed augmentation for prosthetic vision was performed. We qualitatively compared our approach with non-augmented intensity by viewing the output of a prosthetic vision simulator. A given phosphene is computed from a sampled pixel value i in $[0, 255]$ in the image. It is then quantised to the required output dynamic range d (in this case 3 bits) over the range $[0, 255]$ giving the value ($[\cdot]$ denotes the rounding function) $I = \left[\left[i\frac{2^d-1}{255}\right]\frac{255}{2^d-1}\right]$. A discrete unnormalised Gaussian kernel G of standard deviation $\sigma = I^\beta$ and size $w \times w$, $w = \lfloor 6\sigma \rfloor$. The phosphene is then given by the function

$$p[x, y] = \frac{255}{C}\frac{e^\alpha}{\alpha^2}\left(\frac{I_\gamma}{255}\right)^\beta G[x, y],$$

where $x, y \in \left[-\frac{w-1}{2}, \frac{w-1}{2}\right]$, $I_\gamma = 255\left(\frac{I}{255}\right)^\gamma$ $\alpha = (I_\gamma)^\beta$, and C is a normalising constant. The values of β and γ were

Fig. 1. Example frames from the office data set showing from left to right: the original image, the estimated perturbance map and the resulting augmented intensity image.

Fig. 2. Example frames depicting scenarios of daily living showing from left to right: the original image, the estimated perturbance map and the resulting augmented intensity image.

obtained experimentally and fixed for the given output resolution.

Figure 3 shows the resulting phosphene visualisation of the original image using non-augmented intensity (middle column), and our proposed augmentation (right column). The phosphene visualisations are displayed using 98 phosphenes arranged in a hexagonal grid. The dynamic range of each phosphene is 8 levels. These settings were chosen to approximate the visual conditions of current retinal prostheses under development [8, 9].

The difference between the two representations is most apparent in conditions of low contrast. The non-augmented phosphene visualisation of the office corridor scene depicted in Fig 3(a) demonstrates a clear issue using intensity alone, with little contrast between the floor and the grey cabinet on the left. The augmented intensity, however, provides a clear distinction between the floor, and surfaces on either side. The cafe scene in Fig 3(b) also demonstrates how augmentation provides a clearer distinction between the free space in the scene, and the obstructed space. Figures 3(c) and (d) show examples of the augmented intensity providing clear cues to hazardous scenarios such as the edge of the open door in (c), and the drop-off in (d). While the non-augmented intensity provides some evidence of the hazards, the relative importance of the door edge in (c), and the exact point of drop-off in (d) is not conveyed in the visualisation using intensity alone. Figure 3(e) demonstrates how the visual representation may be used to highlight objects of interest on a tabletop.

4. DISCUSSION

The proposed visual representation aims to enhance structurally significant features in the scene to improve functional outcomes for visual prosthesis recipients. These preliminary results demonstrate how these enhancements may support basic way-finding and obstacle avoidance, as well as object location tasks, in a range of common indoor scenarios where high contrast does not always mark surface boundaries. The approach is different to previously proposed augmentations in that it combines two orthogonal descriptions of the scene (*i.e.*, image intensity and the perturbance map) without explicit cueing such as [14], or the global replacement of intensity with depth such as [19]. The proposed augmentation may also be adaptively applied by weighting the perturbance contribution by the level of local constrast in the scene. For example, the perturbance weighting may be reduced when it

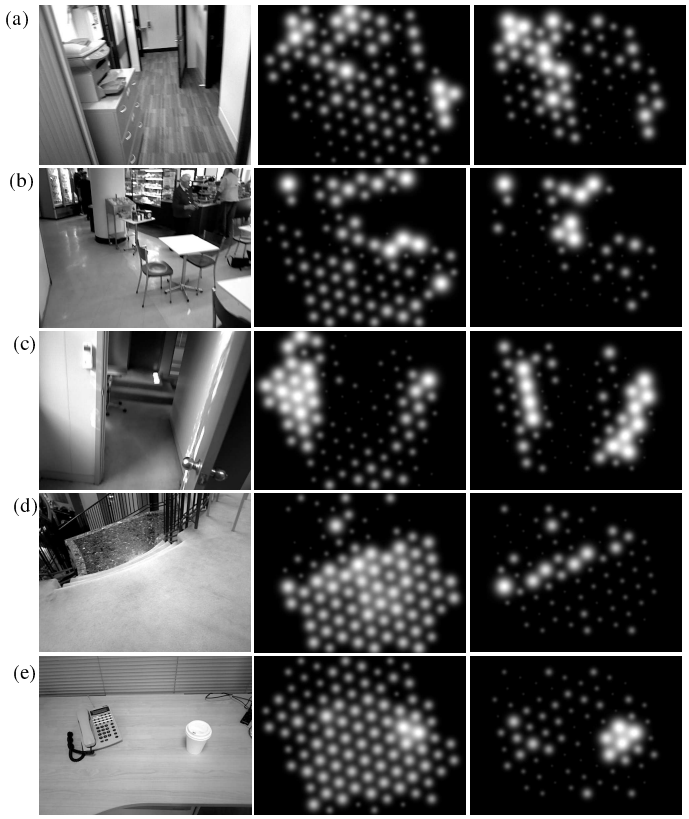

Fig. 3. Example frames with corresponding visualisations in simulated prosthetic vision, showing from left to right: (a) the original image, (b) non-augmented intensity and (c) augmented intensity on a 98 hexagonal phosphene grid. All phosphene images are rendered with a dynamic range of 8 brightness levels.

is clear that intensity edges already mark the structure. Ultimately this balance is dependent on the display constraints of the stimulating implant, and requires further empirical investigation.

We acknowledge that human trials are required to accurately evaluate the effectiveness of the proposed visual representation. However, previous SPV mobility studies using augmentations to emphasise obstacles (*e.g.*, [21, 22]) do provide some guidance. These studies show that subjects were able to make use of augmented visual representations to achieve improved collision rates compared with non-augmented intensity. Measurable improvements over time were also observed. Given the proposed scheme provides similar emphasis of obstacles in the scene (particularly to that of [21]), we expect the proposed augmented-intensity to provide comparable results, with the potential to extend to other tasks of daily living.

The prosthetic vision simulator used in this paper can only approximate what patients perceive with a retinal implant, and does not attempt to capture specific features and characteristics such as shape, size and duration of induced phosphenes (*e.g.*, [23, 9, 8]). Rather, the SPV system provides an abstraction from the significant variability of these reported perceptions. While human trials with real implantees must be conducted to confirm such results, the use of idealised phosphene models provides a generalisable and repeatable means of evaluating the fitness for purpose of vision algorithms and visual representations for prosthetic vision.

5. CONCLUSION

We have proposed a novel visual representation for prosthetic vision that emphasises scene structure in an intensity-based visual representation. By combining the output of a depth-based surface orientation *perturbance map* with the corresponding intensity image, we have demonstrated how the output intensity image can be modified to ensure structural features such as wall-floor boundaries, steps, drop-offs and table top items are distinguishable from surrounding surfaces. Our results suggest particular advantages may be gained using the proposed visual representation over non-augmented intensity with current and near-term visual prostheses. Further work is required to assess the effectiveness of the proposed augmentation through human trialling with real and simulated prosthetic vision.

6. REFERENCES

[1] J.F. Rizzo, J. Wyatt, J. Loewenstein, S. Kelly, and D. Shire, "Perceptual efficacy of electrical stimulation of human retina with a microelectrode array during short-term surgical trials," *Investigative ophthalmology & visual science*, vol. 44, no. 12, pp. 5362–5369, 2003.

[2] J.F. Rizzo III, "Update on retinal prosthetic research: the boston retinal implant project," *Journal of Neuro-Ophthalmology*, vol. 31, no. 2, pp. 160, 2011.

[3] M S. Humayun, J D. Dorn, L Da. Cruz, G. Dagnelie, J-A. Sahel, P E. Stanga, A V. Cideciyan, J L. Duncan, D. Eliott, E. Filley, A C. Ho, A. Santos, A B. Safran, A. Arditi, L V. Del Priore, and R J. Greenberg, "Interim results from the international trial of second sight's visual prosthesis," *Investigative Ophthalmology*, vol. 119, no. 4, pp. 779–788, 2012.

[4] E. Zrenner, K U. Bartz-Schmidt, H. Benav, D. Besch, A. Bruckmann, V-P. Gabel, F. Gekeler, U. Greppmaier, A. Harscher, S. Kibbel, J. Koch, A. Kusnyerik, T. Peters, K. Stingl, H. Sachs, A. Stett, P. Szurman, B. Wilhelm, and R. Wilke, "Subretinal electronic chips allow blind patients to read letters and combine them to words," *Proceedings of the Royal Society B: Biological Sciences*, vol. 278, no. 1711, pp. 1489–1497, 2011.

[5] K.J. Wu, C. Zhang, W.C. Huang, L.M. Li, and Q.S. Ren, "Current research of c-sight visual prosthesis for the blind," in *Engineering in Medicine and Biology Society (EMBC), 2010 Annual International Conference of the IEEE*, 31 2010-sept. 4 2010, pp. 5875 –5878.

[6] E. Zrenner, "Will retinal implants restore vision?," *Science*, vol. 295, pp. 10221025, 2002.

[7] GS Brindley and WS Lewin, "The sensations produced by electrical stimulation of the visual cortex," *The Journal of Physiology*, vol. 196, no. 2, pp. 479, 1968.

[8] M S Humayun, J Weiland, G Y Fujii, R Greenberg, R Williamson, J Little, B Mech, V Cimmarusti, G Van Boemel, G Dagnelie, and E deJuan Jr, "Visual perception in a blind subject with a chronic microelectronic retinal prosthesis," *Vision Research*, vol. 43, pp. 2573–2585, 2003.

[9] D Nanduri, MS Humayun, RJ Greenberg, MJ McMahon, and JD Weiland, "Retinal prosthesis phosphene shape analysis," in *Engineering in Medicine and Biology Society, 2008. EMBS 2008. 30th Annual International Conference of the IEEE*. IEEE, 2008, pp. 1785–1788.

[10] Kichul Cha, Kenneth W. Horch, and Richard A. Normann, "Mobility performance with a pixelized vision system," *Vision Research*, vol. 32, no. 7, pp. 1367 – 1372, 1992.

[11] G. Dagnelie, P. Keane, V. Narla, L. Yang, J. Weiland, and M. Humayun, "Real and virtual mobility performance in simulated prosthetic vision," *Journal of Neural Engineering*, vol. 4, pp. S92–S101, 2007.

[12] Dowling. J A. and A J. Maeder, "Mobility enhancement and assessment for a visual prosthesis," in *SPIE Medical Imaging 2004: Physiology, Function, and Structure from Medical Images*. 2004, International Society for Optical Engineering.

[13] J. Dowling, W. Boles, and A. Maeder, "Mobility assessment using simulated artificial human vision," in *Proceedings of the 2005 Workshop on Computer Vision Applications for the Visually Impaired (CVAVI)*, june 2005.

[14] M S. Humayun N. Parikh and J D. Weiland, "Mobility experiments with simulated vision and peripheral cues," in *Proceedings of the Association for Research in Vision and Ophthalmology (ARVO)*, 2010.

[15] M S. Humayun, L. da Cruz, G. Dagnelie, S. Mohand-Said, P. Stanga, R N. Agrawal, and R J. Greenberg, "Interim performance results from the second sight Argus II retinal prosthesis study," in *Proceedings of the Association for Research in Vision and Ophthalmology (ARVO)*, 2010.

[16] N Parikh, L Itti, and J Weiland, "Saliency-based image processing for retinal prostheses," *Journal of Neural Engineering*, vol. 7, no. 1, pp. 016006, 2010.

[17] V. Pradeep, G. Medioni, and J. Weiland, "A wearable system for the visually impaired," in *Engineering in Medicine and Biology Society (EMBC), 2010 Annual International Conference of the IEEE*, 31 2010-sept. 4 2010, pp. 6233 –6236.

[18] N. Barnes, P. Lieby, J.G. Walker, C. McCarthy, V. Botea, and A.F. Scott, "Evaluating depth-based visual representations for mobility in simulated prosthetic vision," in *Proceedings of the Association for Research in Vision and Ophthalmology (ARVO)*, 2012.

[19] C. McCarthy, N. Barnes, and P. Lieby, "Ground surface segmentation for navigation with a low resolution visual prosthesis," in *Proceedings of IEEE EMBC 2011*. IEEE, 2011, pp. 4457–4460.

[20] D. Feng and C.McCarthy, "Enhancing scene structure in prosthetic vision using iso-disparity contour perturbance maps," in *IEEE EMBC 2013*. IEEE, 2013, in press.

[21] C. McCarthy, P. Lieby, J G. Walker, A F. Scott, V. Botea, and N. Barnes, "Low contrast trip hazard avoidance with simulated prosthetic vision," in *Proceedings of the Association for Research in Vision and Ophthalmology (ARVO)*, 2012.

[22] N Parikh, L Itti, M Humayun, and J Weiland, "Performance of visually guided tasks using simulated prosthetic vision and saliency-based cues," *Journal of Neural Engineering*, vol. 10, no. 2, pp. 026017, 2013.

[23] Robert Wilke, Veit-Peter Gabel, Helmut Sachs, Karl-Ulrich Bartz Schmidt, Florian Gekeler, Dorothea Besch, Peter Szurman, Alfred Stett, Barbara Wilhelm, Tobias Peters, et al., "Spatial resolution and perception of patterns mediated by a subretinal 16-electrode array in patients blinded by hereditary retinal dystrophies," *Investigative ophthalmology & visual science*, vol. 52, no. 8, pp. 5995–6003, 2011.